PNAS RESEARCH ARTICLE | EARTH, ATMOSPHERIC, AND PLANETARY SCIENCES

A dry ancient plume mantle from noble gas isotopes

Rita Parai[a,b,1]

Edited by Marc Hirschmann, University of Minnesota, Minneapolis, MN; received January 31, 2022; accepted May 9, 2022

Primordial volatiles were delivered to terrestrial reservoirs during Earth's accretion, and the mantle plume source is thought to have retained a greater proportion of primordial volatiles compared with the upper mantle. This study shows that mantle He, Ne, and Xe isotopes require that the plume mantle had low concentrations of volatiles like Xe and H_2O at the end of accretion compared with the upper mantle. A lower extent of mantle processing alone is not sufficient to explain plume noble gas signatures. Ratios of primordial isotopes are used to determine proportions of solar, chondritic, and regassed atmospheric volatiles in the plume mantle and upper mantle. The regassed Ne flux exceeds the regassed Xe flux but has a small impact on the mantle Ne budget. Pairing primordial isotopes with radiogenic systems gives an absolute concentration of ^{130}Xe in the plume source of ~1.5×10^7 atoms ^{130}Xe/g at the end of accretion, ~4 times less than that determined for the ancient upper mantle. A record of limited accretion of volatile-rich solids thus survives in the He-Ne-Xe signatures of mantle rocks today. A primordial viscosity contrast originating from a factor of ~4 to ~250 times lower H_2O concentration in the plume mantle compared with the upper mantle may explain (a) why giant impacts that triggered whole mantle magma oceans did not homogenize the growing planet, (b) why the plume mantle has experienced less processing by partial melting over Earth's history, and (c) how early-formed isotopic heterogeneities may have survived ~4.5 Gy of solid-state mantle convection.

volatiles | xenon | noble gases | plume | heterogeneity

Significance

Volatiles (like water, carbon, nitrogen, and the noble gases) were delivered to Earth during its accretion. The quantity and nature of accreted volatiles are determined using helium, neon, and xenon isotopes. The portion of Earth's mantle sampled by plumes experienced less processing by partial melting than the upper mantle but also had a lower concentration of Xe at the end of accretion. Based on relationships between Xe and water in accreting materials, the ancient plume source was drier than the upper mantle by a factor of ~4 to 250. The resulting viscosity contrast may have inhibited magma ocean homogenization and contributed to inefficient mixing of the solid mantle and the preservation of ancient isotopic heterogeneities in the modern mantle.

Isotopic heterogeneities that formed in the first ~100 million years of Earth's history persist in the modern mantle (1–5). Proposed physical mechanisms to preserve early-formed heterogeneities have focused on differences in material properties throughout the solid mantle, such as variations in intrinsic density or viscosity reflecting chemical composition or mineralogy (e.g., FeO, SiO_2) (6–8). However, some isotopic signatures originate from before the last giant impact (1, 9, 10). The Moon-forming giant impact is thought to have melted the whole mantle (11, 12), such that these early-formed signatures predate the formation of dense or viscous solid mantle domains. A mechanism is therefore needed to explain how early-formed mantle heterogeneities survived magma ocean mixing during accretion as well as solid mantle convection over Earth's history.

Water has the potential to affect material properties of both silicate magma (13) and the solid mantle (14–17). To assess whether a difference in primordial water content could have contributed to the preservation of heterogeneities from Earth's earliest history, constraints on initial water abundances in different mantle reservoirs are needed. However, absolute constraints on initial mantle abundances of volatiles (e.g., water, nitrogen, carbon, and the noble gases) are difficult to obtain, as mantle reservoirs have experienced extensive degassing and concurrent incorporation of atmospheric volatiles in association with plate tectonics over the past few billion years (18), obscuring the ancient compositions of mantle reservoirs at the end of accretion.

Noble gas isotope ratios and elemental abundances are powerful tracers of volatile accretion and transport among terrestrial reservoirs. Solar, chondritic, and cometary noble gases may all have contributed to terrestrial volatile reservoirs (19). Constraints on contributions from distinct accreted sources come from ratios of stable, nonradiogenic isotopes (called primordial isotopes) of volatile elements (10, 20–25), though ratios of primordial isotopes of different elements may be altered by fractionation during magma ocean outgassing or addition of elementally fractionated atmospheric noble gases through subduction. Noble gas isotope ratios also trace volatile loss: several lithophile radioactive species decay to produce noble gas isotopes on a range of timescales, from extinct short-lived radionuclides such as ^{244}Pu ($t_{1/2}$ = 80.0 My) to long-lived radionuclides like ^{238}U ($t_{1/2}$ = 4.468 Gy). Volatile loss fractionates ratios of lithophile radioactive parent to atmophile daughter, manifesting as variations in the ratios of radiogenic to primordial noble gas isotopes over time. Taken together, primordial and radiogenic noble gases record a wealth of information about Earth's accretion and processing history.

Author affiliations: [a]Department of Earth and Planetary Sciences, Washington University in St. Louis, St. Louis, MO 63130; and [b]McDonnell Center for the Space Sciences, Washington University in St. Louis, St. Louis, MO 63130

Author contributions: R.P. designed research, performed research, analyzed data, and wrote the paper.

The author declares no competing interest.

This article is a PNAS Direct Submission.

[1]Email: parai@wustl.edu.

This article contains supporting information online at http://www.pnas.org/lookup/suppl/doi:10.1073/pnas.2201815119/-/DCSupplemental.

Published July 14, 2022.

Three isotope systems are discussed here: Pu-U-Xe, U-Th-He, and nucleogenic Ne. Spontaneous fission is a minor decay mode for both ^{244}Pu and ^{238}U; each undergoes fission to produce ^{131,132,134,136}Xe in distinct, characteristic proportions. The primary decay mode for ^{238}U is by alpha emission, producing ^{4}He through a decay chain to ^{206}Pb. ^{235}U and ^{232}Th alpha-decay chains also produce ^{4}He. Nuclear reactions between products of (U,Th) decay and target elements in silicate rocks generate ^{21}Ne, dominantly through the ^{18}O(α,n)^{21}Ne and ^{24}Mg(n, α)^{21}Ne reactions in the mantle (26). Thus, coupled production of radiogenic ^{4}He, nucleogenic ^{21}Ne, and fissiogenic ^{131,132,134,136}Xe is expected as U and Th decay in the mantle.

Noble gas isotopes produced by nuclear reactions tell a story when viewed against the backdrop of primordial isotopes. Samples from plume-influenced localities generally exhibit low ratios of radiogenic ^{4}He to primordial ^{3}He and low ratios of nucleogenic ^{21}Ne to primordial ^{22}Ne compared with mid-ocean ridge basalts (MORBs) (27). Variations in these ratios reflect time-integrated (U+Th)/^{3}He and (U+Th)/^{22}Ne, with low ratios in plumes attributed to limited degassing in association with mantle processing by partial melting (27). The Xe isotope system is unique in that fissiogenic Xe isotopes can be interpreted without reference to primordial isotopes. Studies of fissiogenic Xe in mantle-derived samples independently support a less-degassed plume source: a high proportion of fission Xe produced by the extinct radionuclide ^{244}Pu (rather than extant ^{238}U) requires that the plume source has experienced less processing by partial melting over Earth's history compared with the upper mantle (1–3, 28–30).

Mantle Xe isotopes are interpreted as a mixture of the initial Xe from accretion, regassed atmospheric Xe, radiogenic ^{129}Xe, Pu-fission Xe, and U-fission Xe (20, 31, 32). Plume-influenced and MORB mantle Xe compositions are shown in Fig. 1; while there is variability within each category, the plume and MORB mantle Xe signatures and their mixing component breakdowns are distinct (Fig. 1 and *SI Appendix*, Fig. S1). The plume mantle Xe signature indicates a substantial proportion of regassed atmospheric Xe mixing with initial accreted Xe (~95% of ^{130}Xe from regassing) and fissiogenic Xe dominantly from Pu-fission (1, 3). MORB mantle sources also exhibit a large proportion of regassed atmospheric Xe (75 to 88% of ^{130}Xe from regassing), but exhibit fission Xe compositions closer to U-fission Xe (2, 28, 29). Mantle compositions in Xe isotope spaces illustrate plume and MORB systematics and show that a Pu-fission component must contribute to the Iceland source (Fig. 1 and *SI Appendix*, Fig. S1), indicating strong retention of gases that were generated in the first 500 My of Earth's history in the plume mantle.

Here I show that the combined radiogenic He, nucleogenic Ne, and fissiogenic Xe signatures of mantle reservoirs place strict constraints on the absolute abundances and origins of accreted volatiles in Earth's interior, as coupled isotope ratio evolution depends on the initial budgets of primordial He, Ne, and Xe. Mantle primordial isotope ratios are used to determine the mix of solar, chondritic, and regassed atmospheric volatiles in the MORB and plume mantle sources, and the bulk Ne/Xe ratio of regassed atmosphere is determined. A model of coupled He, Ne, and Xe isotopic evolution is constructed to decipher the story of

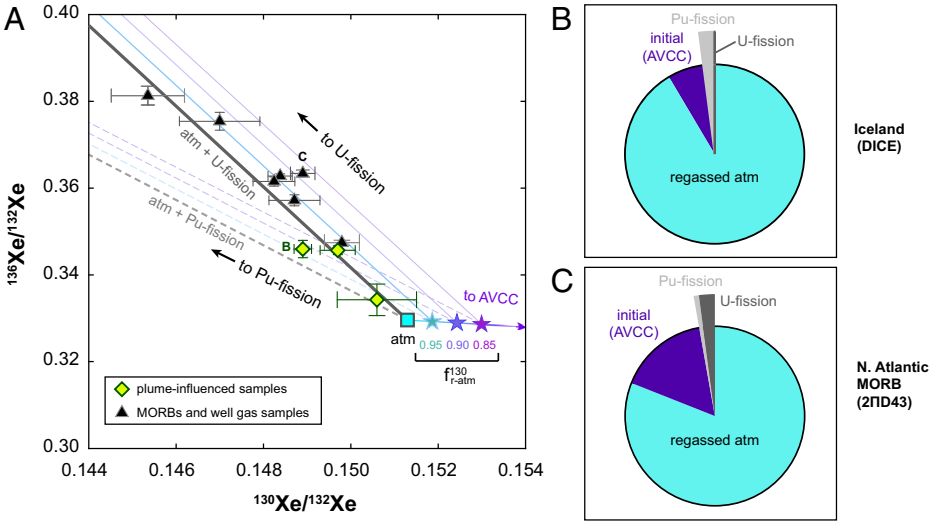

Fig. 1. Xe fission isotope systematics in plume and MORB mantle sources and samples. (*A*) ^{136}Xe/^{132}Xe is plotted against ^{130}Xe/^{132}Xe for plume, MORB, and well gas samples (2σ error bars) (1–3, 20–22, 28–30, 41). Mantle source compositions (corrected for atmospheric contamination) (1–3, 28, 29) are shown along with measurements of screened accumulated gas from step crushing (22, 41) and well gas samples (20, 21, 30). *SI Appendix*, Fig. S1 shows the same components and data in multiple Xe isotope spaces and specifies data sources. The atmospheric composition is shown as a cyan square, and mixing toward the AVCC Xe composition is illustrated with stars marking the proportions of ^{130}Xe from regassed atmosphere (f^{130}_{r-atm} = 0.95, 0.90, and 0.85). Lines showing addition of Pu-fission Xe or U-fission Xe are shown radiating out from the stars, mapping out variable mixtures of the four components in this isotope space. Mixing between atmosphere and U-fission Xe is shown as a bold gray line. Plume compositions indicate a greater proportion of Pu-fission Xe compared with MORB sources and well gases. A given Xe isotopic composition could be explained by a range of mixtures with covariations among mixing components: with a smaller f^{130}_{r-atm}, the mix of Pu- and U-fission Xe tilts toward Pu-fission. However, the range of mixtures to explain a given composition is limited; for instance, no plume composition could be explained with f^{130}_{r-atm} < 0.8. The Iceland (DICE) Xe composition (green diamond marked B) requires a contribution from Pu-fission Xe. Best-fit contributions of ^{132}Xe from regassed atmosphere, initial Xe from accretion, Pu-fission, and U-fission can be determined by linear least squares using multiple Xe isotope ratios (28). (*B* and *C*) Median solutions for component contributions of ^{132}Xe for the Iceland sample DICE (1) and North Atlantic popping rock 2ΠD43 (2) (black triangle marked C in panel *A*). Both mantle sources are dominated by regassed atmospheric Xe contributions. The DICE mantle source Xe composition reflects a higher ratio of regassed atmospheric Xe to initial Xe from accretion (larger f^{130}_{r-atm}), and its fissiogenic Xe signature is dominated by Pu-fission Xe. The 2ΠD43 MORB mantle source Xe composition is consistent with a lower f^{130}_{r-atm} and a stronger U-fission Xe signature. Propagation of uncertainties in Xe isotope ratios gives a range of mixtures that are consistent with a given mantle source composition; these solutions exhibit the covariations described for panel *A*. With propagated uncertainties, the DICE mantle Xe composition still requires a strong contribution from Pu-fission Xe.

accretion and volatile transport recorded in mantle noble gases today, and reveals a dry ancient mantle plume reservoir and a relatively wet upper mantle. The difference in accreted volatile abundances is potentially large enough to generate a viscosity contrast that would inhibit mixing.

Models and Results

Noble gas isotopic evolution models have assumed either (a) a steady-state scenario, where the upper mantle is continuously degassed and replenished by a flux of volatiles from the plume source mantle (33, 34), or (b) similar initial compositions throughout the whole mantle, with divergent evolution for the upper mantle and plume source (35). ^{129}I-^{129}Xe isotope systematics among MORB and plume samples require that the upper mantle and plume reservoir differentiated and acquired distinct I/Xe ratios during the lifetime of ^{129}I (i.e., within the first ~100 My of Earth's history) (1), which rules out the steady-state model and points to early divergence for the two reservoirs.

If MORB and plume mantle reservoirs started with the same initial gas abundances (35) but diverged in their evolution, then two characteristics of the plume Xe isotopic signature would seem in conflict with the high proportion of Pu-fission Xe and the lesser extent of mantle processing for the plume source. First, the proportion of regassed atmospheric Xe in the plume source is similar to or greater than that in the upper mantle (28). The dominant regassed Xe signature in plume sources could only be explained within the framework of an initially homogeneous mantle if recycled material incorporated into the plume source had higher atmospheric Xe concentrations compared with that incorporated into the MORB source, as less recycled material is incorporated into a reservoir with less mantle processing. Second, the Pu-fission Xe excess manifests clearly in the plume source Xe signature (Fig. 1 and *SI Appendix*, Fig. S1), despite retention of a high proportion of the initial gas budget, which would tend to mute fissiogenic excesses relative to the initial composition. It is challenging to reconcile MORB and plume Xe isotope systematics if the whole mantle had a homogeneous initial Xe abundance at the end of accretion and homogeneous abundances of Pu and U. However, the plume source Xe isotopic composition may potentially be explained if the initial abundance of Xe in the plume mantle were low compared with that in the upper mantle.

Part A: Applying a Xe Isotopic Evolution Model to the Plume Mantle. A forward model of mantle Xe isotopic evolution due to degassing, regassing, and fission over Earth's history (18) was adapted to explore the effect of initial Xe abundance and mantle processing history on mantle Xe isotopic signatures. Given an initial mantle Xe isotopic composition (such as average carbonaceous chondrite [AVCC]) (*SI Appendix*), concurrent degassing, ingrowth of fission Xe, and incorporation of regassed atmospheric Xe over Earth's history generate arrays of present-day model outcomes in various Xe isotope spaces (Fig. 2 and *SI Appendix*, Fig. S2).

For a given initial ^{130}Xe abundance ($^{130}Xe_i$), greater extents of mantle processing (high N_{res}) (*SI Appendix*) strongly deplete the accreted initial Xe budget and the Pu-fission Xe, so that regassed atmosphere and U-fission Xe dominate the present-day signature (Fig. 2). A reservoir that experienced little degassing (low N_{res}) retains a greater proportion of its accreted initial Xe and Pu-fission Xe budgets, but the impact of fissiogenic Xe on the total mantle Xe budget depends on $^{130}Xe_i$ and can be muted for high $^{130}Xe_i$ (Fig. 2*B*). Arrays of present-day outcomes that trend toward the Pu-fission Xe component (as needed to explain the Iceland mantle source) are only found for $^{130}Xe_i$ abundances below a certain threshold (Fig. 2*B* and *SI Appendix*, Table S1). This observation places an upper limit on the initial plume mantle Xe abundance associated with the Iceland mantle source composition. Mantle He and Ne isotopic compositions give a lower limit on initial ^{3}He and ^{22}Ne abundances; greater initial abundances can be offset by greater extents of mantle degassing (36). An upper limit initial ^{130}Xe

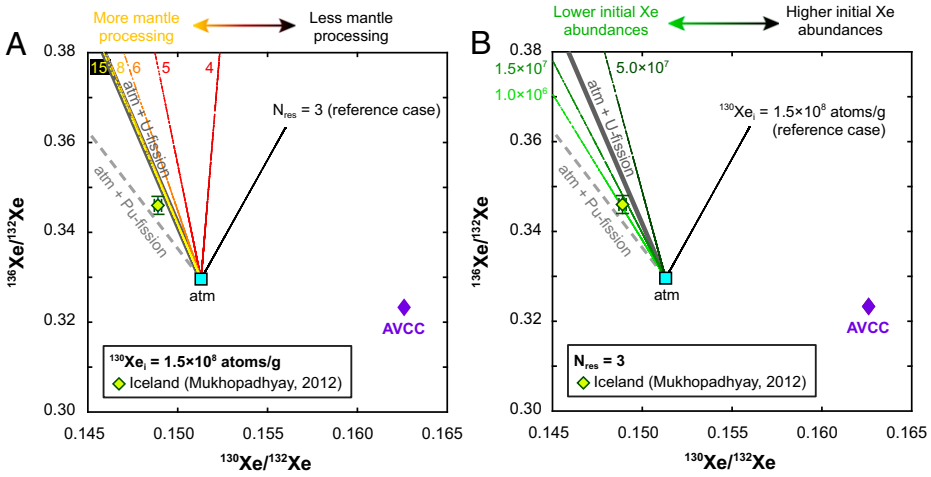

Fig. 2. Xe isotopic evolution modeling to explain the plume Xe signature. Axes are the same as in Fig. 1. Mantle compositions start at AVCC and incorporate fissiogenic and regassed atmospheric Xe over time. Arrays of present-day outcomes radiate from atmosphere, reflecting variable regassed Xe retained in the mantle today. (*A*) The effect of changing the extent of mantle processing given a constant $^{130}Xe_i$. The MORB Xe composition can be modeled using $^{130}Xe_i = 1.5 \times 10^8$ atoms/g and N_{res} of ~7 (18). Reducing N_{res} rotates outcome arrays toward AVCC and cannot explain Iceland Xe (DICE mantle source; green diamond, 2σ). For N_{res} of 3 (reference case), Pu-fission Xe is still retained in the mantle reservoir and the fissiogenic Xe is dominantly from Pu-fission, but fission Xe has a small impact on the overall mantle Xe. Stronger degassing cannot explain the Iceland composition either: higher N_{res} depletes initial Xe and Pu-fission Xe, and arrays rotate toward, but never past, a mixing line between atmospheric and U-fission Xe (see overlap between outcomes for N_{res} of 8 and 15). (*B*) The effect of changing the initial ^{130}Xe concentration given a constant N_{res}. Decreasing $^{130}Xe_i$ rotates arrays away from AVCC. Low $^{130}Xe_i$ can explain Iceland Xe. Above a certain threshold $^{130}Xe_i$ (*SI Appendix*, Table S1), varying N_{res} generates outcomes that fall between atmosphere, U-fission Xe, and AVCC; below that threshold $^{130}Xe_i$, arrays fall between atmosphere, Pu-fission, and U-fission. In both cases, increasing N_{res} rotates the arrays toward the mixing line between atmosphere and U-fission Xe, manifesting as rotation in opposite directions. Plume Xe isotopes require a $^{130}Xe_i$ below the threshold, while $^{130}Xe_i$ must be higher for the MORB mantle (Figs. 1 and 3 and *SI Appendix*).

concentration taken together with lower limit ^{3}He and ^{22}Ne concentrations thus raises the prospect of strict constraints on the absolute abundances and origins of noble gases in the mantle at the end of accretion.

Part B: Using Primordial Isotopes to Decipher Component Mixing. A low initial Xe abundance could reflect ingassed Xe-poor solar nebular volatiles mixing with a limited contribution of volatiles from Xe-rich chondrite material (10, 24). Low Xe/Ne ratios in plume mantle sources compared with the upper mantle support this scenario, as solar nebular gas is characterized by very low Xe/He and Xe/Ne ratios (1–3, 37). Plume ^{20}Ne/^{22}Ne ratios require that solar nebular gas comprises some part of the plume mantle Ne budget (1, 38). Early studies suggested ingassing of solar nebular Ne to Earth's interior, potentially mixed with Ne delivered by accreting solids (36, 39, 40). Williams and Mukhopadhyay (24) noted that Ne-Ar-Xe systematics in MORB and plume-influenced samples are consistent with solar nebular gas mixing with chondritic volatiles or regassed atmospheric volatiles with fractionated elemental ratios and argued that the plume source had incorporated less of the nonsolar volatiles. Relatively low ^{20}Ne/^{22}Ne in the MORB source is therefore due to either a greater contribution from chondrites during accretion or more regassing of atmospheric Ne. The authors did not apportion the nonsolar gas among chondritic and atmospheric contributions, since these two components may have similar primordial noble gas isotope ratios, such as ^{20}Ne/^{22}Ne, ^{36}Ar/^{22}Ne, and ^{130}Xe/^{22}Ne. However, nonsolar gas in the mantle cannot be entirely chondritic, since mantle primordial ^{124,126,128,130}Xe isotopes reflect a significant regassed atmospheric contribution (22). Ne and Xe primordial isotope ratios may be leveraged to constrain mixing proportions of solar nebular, chondritic, and regassed atmospheric primordial isotopes for MORB and plume mantle sources (*SI Appendix*) to pinpoint whether MORB and plume primordial isotope ratios vary as a result of differential regassing or distinct contributions from chondritic material rich in heavy noble gases during accretion.

Solving a system of linear equations describing primordial Ne and Xe isotope ratios yields a greater contribution of ^{22}Ne from chondrites in the MORB source relative to the plume source (~6 versus 0.5%, respectively) (*SI Appendix*, Fig. S3 and Tables S2 and S3). The fraction of ^{22}Ne from atmospheric regassing is also greater in the MORB source (~14 versus ~5% of ^{22}Ne). Thus, a regassing signature from long-term mantle processing is superimposed on a difference from accretion: the MORB mantle started at a lower ^{20}Ne/^{22}Ne (~13) compared with the plume mantle at the end of accretion and experienced more incorporation of regassed atmosphere over time. While the solar contribution dominates Ne budgets in both MORB and plume sources, both mantle Xe budgets are predominantly chondritic primordial Xe mixed with regassed atmospheric Xe due to very low solar ^{130}Xe/^{22}Ne (*SI Appendix*, Tables S2 and S3). The plume mantle Xe isotopic composition at the end of accretion is thus expected to be chondritic rather than solar, consistent with results from Xe in Yellowstone samples (10). Chondritic plume mantle primordial Kr isotopes (10, 41) may likewise be explained by the very low solar ^{84}Kr/^{22}Ne compared with that in chondrites (19).

The computed compositions of regassed atmosphere incorporated into each mantle source over Earth's history (*SI Appendix*, Table S3) indicate that fractionation during the subduction process raises ^{130}Xe/^{22}Ne relative to atmosphere but that the Ne regassing rate is not 0, unlike in the study by Bekaert et al. (42), and exceeds the Xe regassing rate (i.e., ^{130}Xe/^{22}Ne in regassed atmosphere <1 for both MORB and plume compositions). However, the impact of regassing on the mantle Ne isotopic composition is limited because of the higher concentration of Ne in the mantle relative to Xe.

Part C: He-Ne-Xe Coupled Isotopic Evolution Model. The computed mix of primordial He, Ne, and Xe in mantle reservoirs at the end of accretion and the bulk ^{130}Xe/^{22}Ne of regassed atmospheric volatiles set the stage for a forward model of coupled isotopic evolution to determine whether plume and MORB mantle He, Ne, and Xe isotopes can be explained simultaneously, from an estimate of the composition after accretion to the present day (*SI Appendix*, Fig. S4). Free parameters including the initial mantle reservoir ^{130}Xe abundance ($^{130}Xe_i$) and a measure of integrated mantle processing (N_{res}) are explored (*SI Appendix*). Given an initial ^{130}Xe abundance, the budgets of He, Ne, and Xe isotopes at the end of accretion are determined using the computed solar and chondritic primordial isotope mixing proportions. Degassing, regassing, and radiogenic ingrowth proceed according to mantle processing parameters and a growth model for the continental crust. Plume mantle reservoir masses (M_{res}) between 10 and 50% of the mass of the whole mantle are tested; the lower limit corresponds to the estimated present-day mass of large low shear velocity provinces (43), while the upper limit is close to the mass of the mantle below ~1,000 km, where subducting slabs stall (44) and a sudden increase in mantle viscosity has been reported (45). The coupled He-Ne-Xe isotopic evolution of the reservoir is tracked, and present-day model outcomes are compared with plume and MORB mantle compositions (*SI Appendix*, Fig. S4) to calculate residuals (*SI Appendix* and Fig. 3 and *SI Appendix*, Figs. S5 and S6).

The coupled isotopic evolution model succeeds in reproducing present-day mantle He, Ne, and Xe isotopic compositions and abundance ratios for model realizations that pair low integrated mantle processing with low initial ^{130}Xe abundances in the plume source relative to the MORB source (Fig. 3 and *SI Appendix*, Figs. S4–S6). Good fits for all observations are simultaneously achieved (*SI Appendix*, Fig. S7), which was not guaranteed a priori. The good fits indicate that the primordial mix of volatiles determined from Ne and Xe primordial isotopes for each mantle composition succeeds in generating a working model of mantle noble gas accretion, radiogenic He, nucleogenic Ne, fissiogenic Xe, and regassed Ne and Xe contributions. A lower extent of mantle processing (N_{res}) is required for the plume mantle, but this is not sufficient to explain the plume noble gas signature; the initial Xe concentration must also be low in the plume mantle relative to the MORB mantle (Fig. 3). The absolute difference in optimal N_{res} between MORB and plume model reservoirs varies with several parameters (Fig. 3 and *SI Appendix*, Fig. S6), but low $^{130}Xe_i$ in the plume source is robust.

Discussion

The models described above provide constraints on absolute concentrations of volatiles at the end of accretion and on the mix of solar and chondritic volatiles needed to explain plume and MORB signatures (Fig. 4 and *SI Appendix*, Fig. S3). The absolute $^{130}Xe_i$ abundance in the plume reservoir is a free input parameter to the He-Ne-Xe evolution model (part C); the model result of low $^{130}Xe_i$ in the ancient plume mantle is independent but conceptually consistent with the primordial

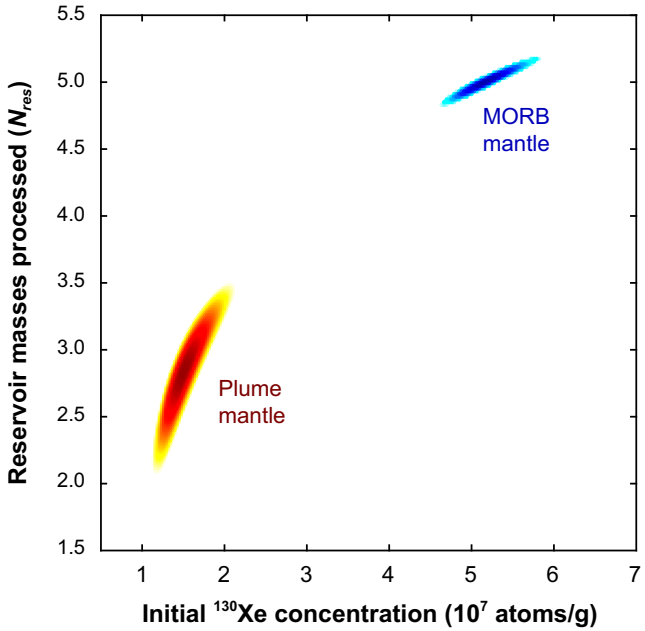

Fig. 3. Map of residuals for plume and MORB He-Ne-Xe isotopic model outcomes. Model outcomes for different combinations of N_{res} and $^{130}Xe_i$ are compared with the DICE and 2ΠD43 compositions for model plume and MORB mantle reservoirs, respectively. The score for a given pairing is the sum of squared sigma-normalized residuals for He, Ne, and Xe isotope ratios (*SI Appendix*, Fig. S5), with Xe isotope ratio residuals weighted double. Only scores <50 are shown in the figure, and the lowest scores (darkest colors) represent the best fits. The isotopic evolution model succeeds in simultaneously reproducing present-day mantle He, Ne, and Xe isotopic and elemental ratios for model realizations that pair low N_{res} with low $^{130}Xe_i$ in the plume source relative to the MORB source. The initial ^{3}He and ^{22}Ne abundances in the plume mantle are higher than those in the MORB mantle because of higher, more solar-like ^{3}He/^{130}Xe and ^{22}Ne/^{130}Xe (*SI Appendix*, Fig. S7 and Table S3). Results are shown for $M_{res} = 2 \times 10^{27}$ g (50% of the mantle) for both mantle reservoirs, accumulation of fissiogenic Xe starting 80 My into Earth's history, and $f^{130}_{r-atm} = 0.95$ and 0.75 for the plume and MORB mantle sources, respectively. The effect of varying model input parameters is shown in *SI Appendix*, Fig. S6. The difference in N_{res} between plume and MORB models shows some limited dependence on input parameters (*SI Appendix*, Fig. S6), but the occurrence of best-fit plume mantle models at low initial $^{130}Xe_i$ is robust. Model outcomes corresponding to the minimum scores are shown compared with DICE and 2ΠD43 compositions in *SI Appendix*, Fig. S7; good fits are simultaneously achieved for He, Ne, and Xe. The plume mantle noble gas signature requires a low initial concentration of Xe as well as less mantle processing than the MORB mantle.

isotope mixing calculation (part B) (*SI Appendix*, Fig. S3) result, which prescribes a smaller proportion of chondritic ^{22}Ne (and thus a lower, more solar-like ^{130}Xe/^{22}Ne) to the plume source at the end of accretion. Evaluation of radiogenic He, nucleogenic Ne, and fissiogenic Xe contributions against primordial isotope budgets thus allows one to peer into the past and observe the initial state of the plume and MORB mantle reservoirs. The best-fit results indicate an initial concentration of ~1.5×10^7 atoms ^{130}Xe/g in the plume mantle, ~4× lower than that in the MORB mantle at the end of accretion (although initial ^{3}He and ^{22}Ne concentrations were higher in the plume mantle) (Fig. 4 and *SI Appendix*, Fig. S7 and Table S3). Prior initial mantle noble gas concentration estimates were lower limits determined assuming closed-system radiogenic ingrowth (e.g., initial ^{3}He) (36); however, initial concentrations could be higher and offset by a greater extent of outgassing over Earth's history to explain a given present-day signature (*SI Appendix*, Fig. S5 *A* and *B*). This is not the case for Pu-U-Xe in the plume mantle: for low $^{130}Xe_i$ concentrations required to explain plume Xe, raising N_{res} does not compensate for a higher $^{130}Xe_i$, as both rotate outcome arrays away from Pu-fission Xe (Fig. 2 and *SI Appendix*, Figs. S2 and S8). Successful reproduction of the plume and MORB mantle He, Ne, and Xe signatures with distinct $^{130}Xe_i$ provides a powerful constraint on the absolute initial Xe concentrations, which can be used to explore the contributions from volatile-rich chondrites to mantle reservoirs through the end of accretion.

Material Contributions from Carbonaceous and Noncarbonaceous Chondrites. The nature of accreted material and the extent of volatile loss during accretion set the initial volatile abundances of mantle reservoirs. Potential contributors of terrestrial volatiles include solar nebular gas dissolved into a magma ocean and retained on the growing Earth, differentiated accreting material, and undifferentiated accreting material. The primordial isotope mixing calculation (part B) (*SI Appendix*, Table S3) indicates that solar nebular gas dominates mantle Ne budgets but makes a negligible contribution of Xe to mantle reservoirs because of its extremely low ^{130}Xe/^{22}Ne ratio. Differentiated materials may have been strongly depleted of volatiles prior to accretion as a result of outgassing and loss to space that occurred on differentiated small bodies; for example, primordial noble gases are absent from the 4.565-My-old achondrite Erg Chech 002 (46). Therefore, undifferentiated materials were likely the dominant source of Xe to the mantle during accretion.

Among undifferentiated materials, carbonaceous chondrites have higher Xe concentrations than noncarbonaceous chondrites. Pristine CM chondrite parent body material is estimated

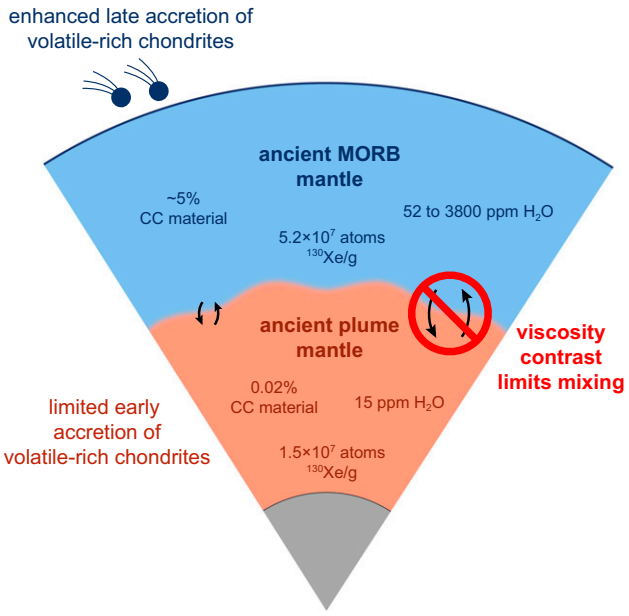

Fig. 4. Plume and MORB mantle reservoirs at the end of accretion. The ancient plume mantle accreted dry, with limited contributions from volatile-rich materials similar to carbonaceous chondrites (CC material). The ancient MORB mantle accreted with a greater mass contribution from volatile-rich material. Estimated Xe and H_2O concentrations are given for both reservoirs at the end of accretion. The plume mantle had a factor of ~4 lower initial ^{130}Xe concentration than the ancient MORB mantle but had higher initial ^{3}He and ^{22}Ne concentrations as a result of higher plume mantle ^{3}He/^{130}Xe and ^{22}Ne/^{130}Xe at the end of accretion (*SI Appendix*, Table S3 and Fig. S7). The present-day MORB and plume mantle reservoirs are internally heterogeneous; it is possible that these reservoirs were already internally heterogeneous at the end of accretion, but additional high-precision isotopic data are needed to assess this possibility. The difference in estimated water contents (ancient plume mantle ~4 to 250× drier than ancient MORB mantle) is large enough to have generated a viscosity contrast that could have limited mixing in a whole mantle magma ocean and may have contributed to inefficient mixing through ~4.5 billion years of solid-state mantle convection.

to have 7.8×10^{10} atoms ^{130}Xe/g (47). In enstatite chondrites, Xe concentrations largely fall in the range from $\sim 1.5 \times 10^{8}$ to $\sim 9.7 \times 10^{9}$ atoms ^{130}Xe/g (48–50), as much as a factor of ~500× lower than the Xe concentration in carbonaceous material. Ordinary chondrites have Xe concentrations that overlap with the lower half of the enstatite chondrite range (51, 52). Mantle primordial Xe isotope ratios are consistent with the average carbonaceous chondrite Xe isotopic composition (10, 22), but enstatite chondrites may have similar Xe isotopic compositions (49) and cannot be ruled out as the source of mantle Xe. However, I note that even very small amounts of pristine carbonaceous materials would dominate mantle Xe budgets at the end of accretion because of their high Xe concentrations.

The mass contributions of undifferentiated carbonaceous or noncarbonaceous material to the growing Earth are explored by assigning the $^{130}Xe_i$ budget of a mantle reservoir entirely to carbonaceous chondrites, entirely to noncarbonaceous chondrites, or to a mixture of both, taking the ranges in ^{130}Xe concentrations for chondritic materials into account (illustrated in *SI Appendix*, Figs. S9 and S10 and summarized in *SI Appendix*, Table S4). It is also necessary to consider when the materials were delivered during the accretion process: delivery prior to magma ocean outgassing would translate to greater material contributions from undifferentiated materials, as some portion of the accreted Xe budget would have been lost through outgassing. Retention of ~1.4% of the accreted Xe budget throughout magma ocean outgassing is explored here; the derivation of this estimate is given in the section below on Xe and H_2O.

The relatively low $^{130}Xe_i$ determined for the ancient plume mantle reservoir compared with Xe concentrations in undifferentiated materials (*SI Appendix*, Table S4) suggests limited accretion of volatile-rich materials. The plume ^{3}He/^{22}Ne ratio at the end of accretion (excluding regassed ^{22}Ne) is elevated by a factor of ~2 compared with the solar ratio (*SI Appendix*, Table S3); such elevation has been interpreted as evidence that the plume mantle experienced one magma ocean episode in equilibrium with a solar nebular atmosphere (9). The entire budget of $^{130}Xe_i$ in the ancient plume mantle could be accounted for with only ~0.02% of plume mantle mass from pristine carbonaceous material accreted after magma ocean crystallization (*SI Appendix*, Fig. S9 and Table S4). Accretion of nearly 100% of plume reservoir mass from Xe-poor ordinary and enstatite chondrites prior to magma ocean outgassing would provide only ~15% of $^{130}Xe_i$; the balance could be delivered by <0.02% mass from pristine carbonaceous materials after magma ocean crystallization (or ~1% mass prior to magma ocean crystallization) (*SI Appendix*, Fig. S9). The ancient plume mantle $^{130}Xe_i$ budget could alternatively be explained by accretion of entirely Xe-poor ordinary or enstatite chondrite-like material, with ~9% mass delivered after magma ocean crystallization; this is the only scenario in which Xe-poor enstatite or ordinary chondrites would contribute significantly to the mantle Xe budget (*SI Appendix*, Figs. S9 and S10 and Table S4) and would require negligible Xe delivery to the plume mantle by carbonaceous material.

The ancient MORB mantle likely experienced multistage volatile loss through multiple giant impacts (9). Some end-member scenarios to explain the MORB mantle $^{130}Xe_i$ budget are explored. Assuming ~1.4% of any pre-giant impact Xe budget is retained in the impact-induced magma ocean, any undifferentiated material accreted prior to the penultimate giant impact experienced >99.98% outgassing and is unlikely to contribute to the MORB mantle budget at the end of accretion. If MORB mantle Xe were primarily delivered between the penultimate and last giant impact, a contribution of ~4.9% of MORB mantle mass from pristine carbonaceous material would account for the estimated $^{130}Xe_i$ (*SI Appendix*, Fig S10 and Table S4). Alternatively, a 39% mass contribution from the most Xe-rich enstatite chondrites delivered between the last two giant impacts could account for the entire MORB mantle $^{130}Xe_i$. Delivery of ordinary chondrites and Xe-poor enstatite chondrites could not account for more than ~4% of MORB mantle $^{130}Xe_i$ (*SI Appendix*, Fig. S10).

Smaller amounts of undifferentiated material could have been delivered entirely after the last giant impact as part of the late veneer, the ~0.5 to 1% of Earth's mass that accreted after metal-silicate equilibration in the last magma ocean. MORB mantle $^{130}Xe_i$ could be explained by late accretion of 0.07% of MORB mantle mass from pristine carbonaceous material or 0.54% of mass from Xe-rich enstatite chondrite material. However, delivery of upper mantle volatiles entirely through the late veneer is inconsistent with the upper mantle hydrogen-nitrogen-carbon abundance pattern, which does not match that of any chondrites (19, 53). Upper mantle volatiles likely reflect fractionation during accretionary impacts and thus were likely delivered during the main phase of accretion (9). In this case, the late veneer that delivered highly siderophile elements to Earth's mantle cannot have added significant Xe to the mantle. Either the late veneer was largely made of ordinary or Xe-poor enstatite chondrite material (a 1% mass contribution of Xe-poor ordinary or enstatite chondrites provides only 3% of MORB mantle $^{130}Xe_i$) (*SI Appendix*, Fig. S10 and Table S4), or late veneer volatiles entered the atmosphere upon accretion.

Lithophile and siderophile stable isotope systematics observed among meteorites and terrestrial samples suggest that ~5% of Earth's mantle mass is from carbonaceous chondrites (54, 55). This estimate is consistent with delivery of MORB mantle Xe via pristine carbonaceous material prior to the last giant impact (*SI Appendix*, Table S4). I note that the bulk silicate Earth Mo isotopic composition lies between parallel trends for noncarbonaceous and carbonaceous chondrites in Mo isotope spaces (56). If initial Xe budgets for the plume and MORB mantle reservoirs originate largely from delivery of Xe-rich carbonaceous material, then this study predicts that among terrestrial samples, Mo isotopes in MORBs would lie closer to the carbonaceous trend than plume samples.

Abundances of Water in Ancient Mantle Reservoirs. Initial Xe abundances can be linked to initial H_2O abundances with some caution. Solar nebular gas is not a significant contributor of mantle Xe (*SI Appendix*), but ingassed nebular H_2 may have been oxidized to generate nebula-derived H_2O in an early magma ocean (57). However, mantle D/H ratios are consistent with chondritic contributions (58–60). In the discussion below, I assume that nebular H_2O is a negligible component in the total mantle H_2O budget.

The abundance of H_2O in mantle sources at the end of accretion can be estimated based on $^{130}Xe_i$ concentrations, the $H_2O/^{130}$Xe ratio in undifferentiated materials, and considerations of fractionation during magma ocean degassing. A compilation of Xe concentrations and $H_2O/^{130}$Xe ratios indicates that while carbonaceous and enstatite chondrites have distinct Xe concentrations, their $H_2O/^{130}$Xe ratios overlap (*SI Appendix*, Fig. S11). Similar $H_2O/^{130}$Xe ratios in carbonaceous and noncarbonaceous chondrites suggest that an estimate of the amount of H_2O delivered in association with Xe is insensitive to the mix of chondritic materials that delivered these volatiles during accretion. The $H_2O/^{130}$Xe ratio estimated for pristine carbonaceous material (47, 61) is similar to the average $H_2O/^{130}$Xe in enstatite

chondrites (49, 50, 60) (*SI Appendix*, Fig. S11) and is adopted here to calculate the amount of H_2O associated with Xe delivered by undifferentiated material.

The strongest contrast in ancient plume and MORB mantle H_2O concentrations would be generated if undifferentiated material were added to the plume source after the magma ocean episode that affected its volatile budgets (9), if undifferentiated material were added to the MORB mantle prior to the last giant impact, and if H_2O were retained preferentially relative to Xe in magma oceans because of its higher solubility (62). If undifferentiated material were added to the plume mantle after its magma ocean episode, the estimated 1.5×10^7 atoms ^{130}Xe/g and an unfractionated chondritic $H_2O/^{130}$Xe (*SI Appendix*, Fig. S11) would yield 15 ppm H_2O in the ancient plume source, drier than the most depleted MORB mantle today (63). An unfractionated chondritic $H_2O/^{130}$Xe and 5.2×10^7 atoms ^{130}Xe/g would give 52 ppm H_2O in the ancient MORB mantle; this is the abundance of H_2O if all chondritic material were added as part of the late veneer, or if the material were added before the last giant impact and H_2O/Xe were not fractionated by magma ocean outgassing (e.g., if kinetic effects made Xe degassing inefficient). If all of the ^{130}Xe in the MORB mantle at the end of accretion were instead residual to equilibrium degassing of a magma ocean in the aftermath of the last giant impact, the ratio of H_2O to Xe could be elevated relative to the chondritic ratio by $>10^4$ based on the large difference in solubility in silicate melts (62, 64). However, the concentration of ^{130}Xe in the MORB mantle at the end of accretion is too high to be residual to equilibrium degassing of a magma ocean with such a large contrast in solubility; the corresponding H_2O contents are not tenable (i.e., >50 wt. % H_2O). Therefore, the ancient MORB mantle H_2O/Xe ratio cannot have been very strongly elevated relative to chondritic, and the last giant impact cannot have driven equilibrium degassing of volatile species dissolved in the last magma ocean, suggesting either limited diffusion of Xe into rapidly rising CO_2 bubbles (the major volatile species that would exsolve from the shallow magma ocean) or low CO_2 contents in the magma ocean generated by the last giant impact.

A reasonable maximum H_2O abundance in the MORB mantle at the end of accretion can be estimated by assuming the MORB mantle carried all of the H_2O that is presently distributed among the modern ocean, the present-day MORB mantle with ~100 ppm H_2O, and a water-rich transition zone (1.5 wt. % H_2O for 10% of the mass of the mantle) (65). Assigning all of this water to the ancient MORB mantle would correspond to 3,800 ppm H_2O, meaning that ancient MORB H_2O/Xe ratios were not elevated by magma ocean outgassing by more than a factor of ~73 relative to the chondritic ratio. An estimate of Xe retention in a magma ocean can be computed by assuming H_2O was retained completely; in this case, a factor of ~73 elevation of the $H_2O/^{130}$Xe ratio is achieved with ~1.4% of Xe retained through magma ocean outgassing, consistent with prior estimates from noble gases (66).

The strongest possible contrast in H_2O abundances that is consistent with the global H_2O budget is thus estimated to be a factor of ~250, with 15 ppm H_2O in the ancient plume mantle and 3,800 ppm H_2O in the ancient MORB mantle (Fig. 4). Such a low initial primordial H_2O concentration in the plume mantle indicates that the present-day estimated 400 to 1,000 ppm in the plume source (63) is either due to regassing or mixing with water-rich material entrained as plumes rise through the transition zone. Stronger net degassing of the MORB mantle over Earth's history may explain the low present-day average H_2O concentrations compared with those in the plume mantle (63).

Preservation of Ancient Isotopic Heterogeneities in the Mantle. The survival of accreted-volatile heterogeneity in the mantle indicated by long-lived radiogenic He, nucleogenic Ne, and fissiogenic Xe noble gas signatures (Figs. 3 and 4) in this study is consistent with the persistence of early-formed (>4.45 Ga) ^{129}I-^{129}Xe isotopic heterogeneities in the mantle today (1–3, 28, 29). The contrast in plume and MORB mantle $^{130}Xe_i$ abundance does not depend on any finely tuned modeling parameter (*SI Appendix*, Fig. S6) and strengthens a dynamic constraint on accretion (9): regardless of the timescale of accretion, a mode of planetary accretion that does not homogenize the growing planet is required.

The result simultaneously provides a physical mechanism to explain such inefficient mixing and the survival of early-formed mantle isotopic heterogeneities. The ancient plume mantle was ~4 to 250× drier than the ancient MORB mantle. An order of magnitude difference in water content can generate a >10× difference in viscosity in silicate melts (13, 67) and in solid silicate (14, 68), which is sufficient to inhibit mixing and preserve heterogeneities over billion-year timescales (69). The plume mantle has experienced significant processing and incorporation of recycled slabs and is not a primordial mantle reservoir (31). However, a higher viscosity may explain why the plume mantle experienced less processing and retained a greater proportion of its initial volatile budget than the MORB mantle (Fig. 3) over Earth's history. If plumes originate from the mantle below ~1000 km, a decrease in mantle water contents could contribute to the abrupt increase in viscosity in the midmantle (45), in which case high present-day plume H_2O concentrations would reflect entrainment of water-rich material during plume ascent, potentially from the transition zone. However, plume noble gas isotopes are equally consistent with a smaller plume mantle reservoir (~10% of the mass of the mantle, consistent with large low shear velocity provinces) (43) (*SI Appendix*, Fig. S6*C*) with 400 to 1,000 ppm H_2O resulting from regassing. Independent of the location of the plume source in the mantle, an ancient viscosity contrast reflecting a difference in H_2O concentration may have limited direct mixing of the ancient plume and MORB mantle reservoirs during whole mantle magma ocean episodes and may have contributed to inefficient mixing throughout ~4.5 billion years of solid-state mantle convection.

Materials and Methods

A numeric model of mantle He, Ne, and Xe isotopic evolution was used to explore a parameter space and identify combinations of input parameters that could explain the He, Ne, and Xe isotopic compositions and elemental abundances in the Iceland mantle source (1) and North Atlantic MORB mantle (2). The model input parameters, notes on the published data used in calculations, and equations used for modeling are given in the *SI Appendix*.

In model part A, a Xe isotopic evolution model adapted and expanded from Parai and Mukhopadhyay (18) was used to explore the effect of the mantle processing rate history (parameterized as N_{res}) and initial Xe concentrations on present-day mantle Xe isotopic compositions. In model part B, primordial isotope ratios (^{20}Ne/^{22}Ne, ^{130}Xe/^{22}Ne) of mantle sources were treated as linear mixtures between solar, chondritic, and regassed atmospheric Ne and Xe; proportions of ^{22}Ne from each component were determined after accounting for the proportion of ^{130}Xe from regassing and under the constraint that the proportions must sum to 1. In model part C, the results from part B were used to compute the abundances and isotopic compositions of He, Ne, and Xe in mantle reservoirs at the end of accretion. A forward model of degassing, regassing, and ingrowth through nuclear reactions (*SI Appendix*, Fig. S4) was used to determine

present-day mantle reservoir He, Ne, and Xe isotopic compositions and elemental abundance ratios. These were compared with mantle source compositions for the Icelandic sample DICE (1) and the North Atlantic MORB 2ΠD43 (2), and sums of squared residuals (normalized to uncertainties in the mantle source compositions) were computed for different combinations of input parameters.

The contributions from chondritic materials during accretion were computed by attributing the initial ^{130}Xe concentration ($^{130}Xe_i$) of a mantle reservoir to delivery by a mixture of carbonaceous and noncarbonaceous materials during accretion. As shown in *SI Appendix*, Figs. S9 and S10, the proportion of $^{130}Xe_i$ from carbonaceous materials was varied from 0 (entirely noncarbonaceous source of mantle initial Xe) to 1 (entirely carbonaceous source). Multiplying $^{130}Xe_i$ by the fractional proportion of ^{130}Xe from carbonaceous materials gave the concentration of mantle ^{130}Xe from carbonaceous material at the end of accretion. The balance of $^{130}Xe_i$ was attributed to noncarbonaceous material. Material contributions were determined for two scenarios: delivery prior to and during magma ocean outgassing or delivery after magma ocean crystallization. For delivery after magma ocean crystallization (*SI Appendix*, Figs. S9*A* and S10*B*), material contributions were computed by dividing the carbonaceous or noncarbonaceous $^{130}Xe_i$ concentration in the mantle reservoir by the concentration in the accreting material. For delivery prior to and during magma ocean outgassing (*SI Appendix*, Figs. S9*B* and S10*A*), I assumed ∼1.4% of delivered Xe was retained in the residual magma ocean (see above), consistent with the estimate from Porcelli et al. (66). The ancient mantle ^{130}Xe concentration prior to outgassing was computed by multiplying by ∼73 (equivalent to dividing out ∼0.014), and the resulting concentration was divided by the concentration of ^{130}Xe in carbonaceous or noncarbonaceous material to give material contributions.

For carbonaceous chondrites, upper and lower bounds on the concentration of Xe were taken from a study of a large set of CM chondrites (47). The bounds corresponded to the maximum Xe concentration estimated for pristine carbonaceous materials and the minimum estimated for aqueously altered materials. Compared with carbonaceous materials, enstatite and ordinary chondrites are both characterized by lower Xe concentrations overall, but the maximum Xe concentration in enstatite chondrites is higher than that in ordinary chondrites. *SI Appendix*, Figs. S9 and S10 show the bounds on noncarbonaceous material contributions calculated by adopting the highest enstatite chondrite Xe concentration and the lowest Xe concentration in enstatite and ordinary chondrites.

Concentrations of H_2O in ancient mantle reservoirs were computed by multiplying the initial ^{130}Xe concentration ($^{130}Xe_i$) by an $H_2O/^{130}$Xe ratio of 10^{-10} (wt. % H_2O)/(atoms ^{130}Xe/g), which corresponds to a molar $H_2O/^{130}$Xe ratio of $\sim 3.3 \times 10^{10}$. This is the ratio computed for pristine carbonaceous materials based on the relationship evident in *SI Appendix*, Fig. S11*A* and is similar to the average $H_2O/^{130}$Xe ratio for enstatite chondrites (*SI Appendix*, Fig. S11*B*). Among CM chondrites, aqueously altered chondrites have lower Xe concentrations than pristine chondrites but have similar H_2O concentrations (47, 61). It is not clear whether the material available for accreting planets was pristine or aqueously altered. If Xe were delivered to Earth's interior by carbonaceous material strongly affected by aqueous alteration prior to accretion, then the appropriate $H_2O/^{130}$Xe ratio would be 5× higher (*SI Appendix*, Fig. S11). This would increase the ancient plume H_2O estimate from 15 to 75 ppm. It is also possible that the $H_2O/^{130}$Xe ratio in the most Xe-rich enstatite chondrites is lower than the value adopted above. If Xe were delivered to Earth's interior by Xe-rich enstatite chondrites, using the lowest $H_2O/^{130}$Xe in enstatite chondrites would yield 7 ppm H_2O in the ancient plume mantle. However, in either case, the upper limit for MORB mantle H_2O would still be 3,800 ppm, calculated through mass balance. The contrast in mantle H_2O concentrations therefore would either fall within the ∼4 to 250× range given in the main text or would be even stronger.

Data Availability. MATLAB code data have been deposited in the Github repository (https://github.com/ritaparai/DryAncientPlume) (70).

ACKNOWLEDGMENTS. This work was supported by Department of Energy National Nuclear Security Administration Grant DENA003911 to R.P. I thank Slava Solomatov and Bruce Fegley for discussions on pertinent topics. I thank the editor for efficient handling, and am grateful to David Fike, Douglas Wiens, Vedran Lekic, Julian Rodriguez, and two anonymous reviewers for comments that improved the manuscript.

1. S. Mukhopadhyay, Early differentiation and volatile accretion recorded in deep-mantle neon and xenon. *Nature* **486**, 101–104 (2012).
2. R. Parai, S. Mukhopadhyay, Heavy noble gas signatures of the North Atlantic Popping Rock 2ΠD43: Implications for mantle noble gas heterogeneity. *Geochim. Cosmochim. Acta* **294**, 89–105 (2021).
3. M. K. Pető, S. Mukhopadhyay, K. A. Kelley, Heterogeneities from the first 100 million years recorded in deep mantle noble gases from the Northern Lau Back-arc Basin. *Earth Planet. Sci. Lett.* **369**, 13–23 (2013).
4. A. Mundl *et al.*, Tungsten-182 heterogeneity in modern ocean island basalts. *Science* **356**, 66–69 (2017).
5. H. Rizo *et al.*, Preservation of Earth-forming events in the tungsten isotopic composition of modern flood basalts. *Science* **352**, 809–812 (2016).
6. M. D. Ballmer, C. Houser, J. W. Hernlund, R. M. Wentzcovitch, K. Hirose, Persistence of strong silica-enriched domains in the Earth's lower mantle. *Nat. Geosci.* **10**, 236 (2017).
7. S. Labrosse, J. W. Hernlund, N. Coltice, A crystallizing dense magma ocean at the base of the Earth's mantle. *Nature* **450**, 866–869 (2007).
8. A. J. Gülcher, D. J. Gebhardt, M. D. Ballmer, P. J. Tackley, Variable dynamic styles of primordial heterogeneity preservation in the Earth's lower mantle. *Earth Planet. Sci. Lett.* **536**, 116160 (2020).
9. J. M. Tucker, S. Mukhopadhyay, Evidence for multiple magma ocean outgassing and atmospheric loss episodes from mantle noble gases. *Earth Planet. Sci. Lett.* **393**, 254–265 (2014).
10. M. W. Broadley *et al.*, Identification of chondritic krypton and xenon in Yellowstone gases and the timing of terrestrial volatile accretion. *Proc. Natl. Acad. Sci. U.S.A.* **117**, 13997–14004 (2020).
11. S. J. Lock, S. T. Stewart, M. Ćuk, The energy budget and figure of Earth during recovery from the Moon-forming giant impact. *Earth Planet. Sci. Lett.* **530**, 115885 (2020).
12. M. Nakajima, D. J. Stevenson, Melting and mixing states of the Earth's mantle after the Moon-forming impact. *Earth Planet. Sci. Lett.* **427**, 286–295 (2015).
13. H. Hui, Y. Zhang, Toward a general viscosity equation for natural anhydrous and hydrous silicate melts. *Geochim. Cosmochim. Acta* **71**, 403–416 (2007).
14. G. Hirth, D. Kohlstedt, Rheology of the upper mantle and the mantle wedge: A view from the experimentalists. *Geophys. Monograph* **138**, 83–106 (2003).
15. S. Mei, D. Kohlstedt, Influence of water on plastic deformation of olivine aggregates: 1. Diffusion creep regime. *J. Geophys. Res. Solid Earth* **105**, 21457–21469 (2000).
16. S. Mei, D. L. Kohlstedt, Influence of water on plastic deformation of olivine aggregates: 2. Dislocation creep regime. *J. Geophys. Res. Solid Earth* **105**, 21471–21481 (2000).
17. V. Solomatov, C. Reese, Grain size variations in the Earth's mantle and the evolution of primordial chemical heterogeneities. *J. Geophys. Res. Solid Earth* **113**, B7 (2008).
18. R. Parai, S. Mukhopadhyay, Xenon isotopic constraints on the history of volatile recycling into the mantle. *Nature* **560**, 223–227 (2018).
19. B. Marty, The origins and concentrations of water, carbon, nitrogen and noble gases on Earth. *Earth Planet. Sci. Lett.* **313**, 56–66 (2012).
20. M. W. Caffee *et al.*, Primordial noble gases from Earth's mantle: Identification of a primitive volatile component. *Science* **285**, 2115–2118 (1999).
21. G. Holland, C. J. Ballentine, Seawater subduction controls the heavy noble gas composition of the mantle. *Nature* **441**, 186–191 (2006).
22. S. Péron, M. Moreira, Onset of volatile recycling into the mantle determined by xenon anomalies. *Geochem. Perspect. Lett.* **9**, 21–25 (2018).
23. E. Füri, B. Marty, Nitrogen isotope variations in the solar system. *Nat. Geosci.* **8**, 515–522 (2015).
24. C. D. Williams, S. Mukhopadhyay, Capture of nebular gases during Earth's accretion is preserved in deep-mantle neon. *Nature* **565**, 78–81 (2019).
25. B. Marty, Meteoritic noble gas constraints on the origin of terrestrial volatiles. *Icarus* **381**, 115020 (2022).
26. G. W. Wetherill, Variations in the isotopic abundances of neon and argon extracted from radioactive minerals. *Phys. Rev.* **96**, 679 (1954).
27. D. W. Graham, Noble gas isotope geochemistry of mid-ocean ridge and ocean island basalts: Characterization of mantle source reservoirs. *Rev. Mineral. Geochem.* **47**, 247–317 (2002).
28. R. Parai, S. Mukhopadhyay, The evolution of MORB and plume mantle volatile budgets: Constraints from fission Xe isotopes in Southwest Indian Ridge basalts. *Geochem. Geophys. Geosyst.* **16**, 719–735 (2015).
29. J. M. Tucker, S. Mukhopadhyay, J. G. Schilling, The heavy noble gas composition of the depleted MORB mantle (DMM) and its implications for the preservation of heterogeneities in the mantle. *Earth Planet. Sci. Lett.* **355**, 244–254 (2012).
30. D. V. Bekaert, M. W. Broadley, A. Caracausi, B. Marty, Novel insights into the degassing history of Earth's mantle from high precision noble gas analysis of magmatic gas. *Earth Planet. Sci. Lett.* **525**, 115766 (2019).
31. R. Parai, S. Mukhopadhyay, J. M. Tucker, M. K. Pető, The emerging portrait of an ancient, heterogeneous and continuously evolving mantle plume source. *Lithos* **346-347**, 105153 (2019).
32. S. Mukhopadhyay, R. Parai, Noble gases: A record of Earth's evolution and mantle dynamics. *Annu. Rev. Earth Planet. Sci.* **47**, 389–419 (2019).
33. L. Kellogg, G. Wasserburg, The role of plumes in mantle helium fluxes. *Earth Planet. Sci. Lett.* **99**, 276–289 (1990).
34. D. Porcelli, G. Wasserburg, Mass transfer of helium, neon, argon, and xenon through a steady-state upper mantle. *Geochim. Cosmochim. Acta* **59**, 4921–4937 (1995).
35. H. M. Gonnermann, S. Mukhopadhyay, Preserving noble gases in a convecting mantle. *Nature* **459**, 560–563 (2009).
36. C. L. Harper, S. B. Jacobsen, Noble gases and Earth's accretion. *Science* **273**, 1814–1818 (1996).
37. M. Moreira, J. Kunz, C. Allegre, Rare gas systematics in popping rock: Isotopic and elemental compositions in the upper mantle. *Science* **279**, 1178–1181 (1998).
38. R. Yokochi, B. Marty, A determination of the neon isotopic composition of the deep mantle. *Earth Planet. Sci. Lett.* **225**, 77–88 (2004).
39. C. Hayashi, K. Nakazawa, Y. Nakagawa, "Formation of the solar system" in *Protostars and Planets II*, D. Black, M. S. Matthews, Eds. (University of Arizona Press, Tucson, AZ, 1985), pp. 1100–1153.

40. H. Hiyagon, M. Ozima, B. Marty, S. Zashu, H. Sakai, Noble gases in submarine glasses from mid-oceanic ridges and Loihi seamount: Constraints on the early history of the Earth. *Geochim. Cosmochim. Acta* **56**, 1301–1316 (1992).
41. S. Péron, S. Mukhopadhyay, M. D. Kurz, D. W. Graham, Deep-mantle krypton reveals Earth's early accretion of carbonaceous matter. *Nature* **600**, 462–467 (2021).
42. D. Bekaert *et al.*, Subduction-driven volatile recycling: A global mass balance. *Annu. Rev. Earth Planet. Sci.* **49**, 37–70 (2021).
43. S. Cottaar, V. Lekic, Morphology of seismically slow lower-mantle structures. *Geophys. J. Int.* **207**, 1122–1136 (2016).
44. Y. Fukao, M. Obayashi, Subducted slabs stagnant above, penetrating through, and trapped below the 660 km discontinuity. *J. Geophys. Res. Solid Earth* **118**, 5920–5938 (2013).
45. M. L. Rudolph, V. Lekić, C. Lithgow-Bertelloni, Viscosity jump in Earth's mid-mantle. *Science* **350**, 1349–1352 (2015).
46. J.-A. Barrat *et al.*, A 4,565-My-old andesite from an extinct chondritic protoplanet. *Proc. Natl. Acad. Sci. U.S.A.* **118**, e2026129118 (2021).
47. D. Krietsch *et al.*, Noble gases in CM carbonaceous chondrites: Effect of parent body aqueous and thermal alteration and cosmic ray exposure ages. *Geochim. Cosmochim. Acta* **310**, 240–280 (2021).
48. J. Crabb, E. Anders, Noble gases in E-chondrites. *Geochim. Cosmochim. Acta* **45**, 2443–2464 (1981).
49. R. Okazaki, N. Takaoka, K. Nagao, T. Nakamura, Noble gases in enstatite chondrites released by stepped crushing and heating. *Meteorit. Planet. Sci.* **45**, 339–360 (2010).
50. A. Patzer, L. Schultz, Noble gases in enstatite chondrites II: The trapped component. *Meteorit. Planet. Sci.* **37**, 601–612 (2002).
51. L. Schultz, H. Weber, F. Begemann, Planetary noble gases in H3-and H4-chondrite falls. *Meteoritics* **25**, 405 (1990).
52. L. Schultz, H. Weber, F. Begemann, Noble gases in H-chondrites and potential differences between Antarctic and non-Antarctic meteorites. *Geochim. Cosmochim. Acta* **55**, 59–66 (1991).
53. A. N. Halliday, The origins of volatiles in the terrestrial planets. *Geochim. Cosmochim. Acta* **105**, 146–171 (2013).
54. K. R. Bermingham, E. Füri, K. Lodders, B. Marty, The NC-CC isotope dichotomy: Implications for the chemical and isotopic evolution of the early solar system. *Space Sci. Rev.* **216**, 133 (2020).
55. N. Dauphas, The isotopic nature of the Earth's accreting material through time. *Nature* **541**, 521–524 (2017).
56. G. Budde, C. Burkhardt, T. Kleine, Molybdenum isotopic evidence for the late accretion of outer Solar System material to Earth. *Nat. Astron.* **3**, 736–741 (2019).
57. M. Ikoma, H. Genda, Constraints on the mass of a habitable planet with water of nebular origin. *Astrophys. J.* **648**, 696 (2006).
58. C. M. O. Alexander, The origin of inner solar system water. *Philos. Trans.- Royal Soc., Math. Phys. Eng. Sci.* **375**, 20150384 (2017).
59. M. W. Loewen, D. W. Graham, I. N. Bindeman, J. E. Lupton, M. O. Garcia, Hydrogen isotopes in high 3He/4He submarine basalts: Primordial vs. recycled water and the veil of mantle enrichment. *Earth Planet. Sci. Lett.* **508**, 62–73 (2019).
60. L. Piani *et al.*, Earth's water may have been inherited from material similar to enstatite chondrite meteorites. *Science* **369**, 1110–1113 (2020).
61. C. M. O. Alexander *et al.*, The provenances of asteroids, and their contributions to the volatile inventories of the terrestrial planets. *Science* **337**, 721–723 (2012).
62. B. Fegley, K. Lodders, N. S. Jacobson, Volatile element chemistry during accretion of the earth. *Geochemistry* **80**, 125594 (2020).
63. R. Parai, S. Mukhopadhyay, How large is the subducted water flux? New constraints on mantle regassing rates. *Earth Planet. Sci. Lett.* **317**, 396–406 (2012).
64. A. Paonita, Noble gas solubility in silicate melts: A review of experimentation and theory, and implications regarding magma degassing processes. *Ann. Geophys.* **48**, 647–669 (2005).
65. H. Fei *et al.*, A nearly water-saturated mantle transition zone inferred from mineral viscosity. *Sci. Adv.* **3**, e1603024 (2017).
66. D. Porcelli, D. Woolum, P. Cassen, Deep Earth rare gases: Initial inventories, capture from the solar nebula, and losses during Moon formation. *Earth Planet. Sci. Lett.* **193**, 237–251 (2001).
67. H. M. Gonnermann, Magma fragmentation. *Annu. Rev. Earth Planet. Sci.* **43**, 431–458 (2015).
68. S.-I. Karato, H. Jung, Effects of pressure on high-temperature dislocation creep in olivine. *Philos. Mag.* **83**, 401–414 (2003).
69. M. Manga, Mixing of heterogeneities in the mantle: Effect of viscosity differences. *Geophys. Res. Lett.* **23**, 403–406 (1996).
70. R. Parai, A dry ancient plume mantle from noble gas isotopes. GitHub. https://github.com/ritaparai/DryAncientPlume. Deposited 3 May 2022.